Journal of Power Sources 240 (2013) 486–493

Contents lists available at SciVerse ScienceDirect

Journal of Power Sources

journal homepage: www.elsevier.com/locate/jpowsour

Manufacturing all-polymer laminar flow-based fuel cells

A.S. Hollinger, P.J.A. Kenis*

Department of Chemical & Biomolecular Engineering, University of Illinois at Urbana-Champaign, 600 S. Matthews Avenue, Urbana, IL 61801, USA

HIGHLIGHTS

- Manufactured a lightweight, all-polymer direct methanol laminar flow fuel cell.
- Bonding strategy eliminates the need for heavy metal plates and clamping.
- Developed a strategy to encapsulate fuel cell electrodes in Kapton windows.
- Designs can be scaled and stacked to achieve power requirements of portable applications.

ARTICLE INFO

Article history:
Received 24 November 2012
Received in revised form
8 April 2013
Accepted 11 April 2013
Available online 19 April 2013

Keywords:
Manufacturing
Polymer
Laminar flow
Microfluidic
Fuel cell
Stack

ABSTRACT

On the macroscale, fuel cell systems typically require heavy clamping constructions to seal layers. Here we report an alternative manufacturing approach that utilizes patterned polymer layers to yield much thinner, lighter laminar flow-based fuel cells (LFFCs). Most LFFCs reported to date have been proof-of-concept configurations. To meet the power requirements of portable electronic devices, challenges related to the design and manufacturing of scalable LFFC systems still need to be addressed. Here we report electrodes that are encapsulated between polymer layers with metallized polymer layers serving as current collectors. Assembly of a polymer-encapsulated anode and cathode yields a 1-mm thick all-polymer fuel cell, about one order of magnitude thinner than most microfluidic fuel cells. To identify performance changes associated with this alternative approach to electrode and catalyst integration, we first validated performance by analyzing the polymer-encapsulated anodes and cathodes individually, and then the complete cell after bonding the polymer-encapsulated electrodes together. This all-polymer fuel cell achieved a maximum power density of 10 mW cm^{-2} at room temperature when using 1 M methanol as the fuel. Thin, lightweight fuel cell stacks for future portable power applications could be obtained by scaling and stacking of the all-polymer cell reported here.

1. Introduction

Significant research effort has focused on developing integrated, multifunctional microchemical systems that incorporate multiple fluidic, electronic, and mechanical components and chemical processes onto a small chip [1–3]. Since their inception, a trend toward increased integration and system complexity has led to the development of highly integrated microsystems for a broad range of applications, including protein crystallization [4], genetic analysis [5,6], multistep synthesis [7], and point-of-care medical diagnostics [8]. Many of these integrated chips are fabricated from polymers, owing to polymers' wide range of material properties, such as mechanical strength, optical transparency, chemical stability, and biocompatibility, which can be tailored to specific applications [9–12]. However, to achieve commercialization of these devices, manufacturing techniques must be advanced in parallel with fluid handling and analytical/chemical capabilities [13]. Here we will address this challenge by developing polymer-based manufacturing technologies, using the assembly of an all-polymer laminar flow-based fuel cell (LFFC) as an example.

LFFCs have been investigated extensively as an alternative to membrane-based fuel cells [14–20]. Most LFFCs reported to date have been proof-of-concept unit cells [18,20]. Transitioning from proof-of-concept, single-channel cells to a multichannel system that provides sufficient power output for portable electronic applications is a present challenge. At the macroscale, fuel cells are traditionally assembled manually in layer-by-layer fashion followed by clamping the layers between metal plates. Scaling to larger systems involves the stacking of an increasing number of layers, requiring increasingly heavy clamping constructions.

Here we report an alternative approach to fuel cell manufacturing which utilizes patterned polymer layers to

* Corresponding author. Tel.: +1 217 265 0523; fax: +1 217 333 5052.
E-mail address: kenis@illinois.edu (P.J.A. Kenis).

0378-7753/$ – see front matter © 2013 Elsevier B.V. All rights reserved.
http://dx.doi.org/10.1016/j.jpowsour.2013.04.053

eliminate the heavy clamping structures needed in traditional fuel cell stacks. This approach will yield much smaller, lighter structures and thinner stacks, which is attractive for portable applications. In prior work with polymer-based fuel cells, Wheldon et al. developed a polyester-laminated, hydrogen/air fuel cell (>1 cm thick) that achieves a maximum power density of 57 mW cm^{-2} at room temperature [21]. Using a different approach, Tominaka et al. hot-embossed cyclic olefin copolymer (COC) to create a 200-μm thick methanol fuel cell [22]. While much thinner, the maximum power density of the COC-based cell is <0.3 mW cm^{-2}.

For the all-polymer fuel cell reported here, polyimide will be used as the substrate. Polyimide has exceptional chemical and thermal stability compared to other polymers, is well-known from IC manufacturing processes, and has previously been used to fabricate microfluidic devices [11,23]. Furthermore, polyimide can be metallized, which is needed for the integration of fuel cell electrodes. As detailed below, we aim to fabricate a thin (mm-thick) polymer-based, methanol fuel cell that achieves power levels sufficient for portable electronic applications.

2. Design

An exploded diagram of the polyimide-based LFFC reported here is shown in Fig. 1. The Kapton sheets used in fabrication of this LFFC are either 50-μm or 125-μm thick, and unless otherwise noted, each layer is 3.5 inches by 2 inches. Working from the left of the schematic, the first layer serves as an anode current collector. This 50-μm thick Kapton layer is metallized for current collection and is machined with inlet and outlet holes for the fuel/electrolyte and oxidant streams. The next layer is a ~190-μm thick carbon paper electrode that has anode catalyst deposited onto the side opposite of the anode current collector. Next, a 50-μm thick Kapton layer encapsulates the anode, leaving a window for fuel/electrolyte to flow over the anode catalyst. Fuel/electrolyte and oxidant streams pass through this layer.

The following channel layer, machined from 125-μm thick Kapton, facilitates the transport of fuel to the anode catalyst. The oxidant stream flows through this layer, while the fuel/electrolyte stream enters this layer on one side, flows laminarly across the layer, and then exits the fuel cell on the opposite side. The next 50-μm Kapton layer encapsulates the cathode, leaving a window for the Nafion layer to conduct the protons produced at the anode. The oxidant passes through this layer. Next is a ~240-μm thick cathodic gas diffusion electrode (GDE); catalyst is deposited on the side opposite the cathode current collector and a Nafion layer is hot-pressed over the catalyst. The subsequent metallized Kapton layer (50-μm thick) is the cathode current collector, which is machined with a window for oxidant transport to the cathodic GDE. Next, a 50-μm thick Kapton layer facilitates oxidant transport to the cathode catalyst. The oxidant stream enters this layer on one side, flows across the layer, and then exits the fuel cell on the opposite side. Lastly, a 50-μm thick Kapton layer seals the oxidant flow channel. The entire 9-layer cell is ~1 mm thick.

Key to the successful assembly of these 9-layer cells is hermetic bonding of all the layers, such that no clamping structures have to be used. All bonding of the layers in these cells was accomplished by using an adhesive in combination with plasma treatment of the surfaces. The details of this step are provided in experimental Section 3.1.

This multi-layer cell design can also be used to create fuel cell stacks. In a stack, the fuel/electrolyte and oxidant streams would exit individual fuel cells in a direction opposite that shown in Fig. 1. The streams would then proceed to the following fuel cell in the stack. The exact configuration and dimensions of electrodes in such multichannel laminar flow-based fuel cell designs will affect performance. In prior work we described detailed design rules for this purpose [24]. For example, shorter and shallower channels, as well as the introduction of herringbone features along the walls in certain locations to enhance boundary layer replenishment, will lead to the desired higher current densities.

3. Experimental

3.1. Kapton fuel cell fabrication

The all-polymer fuel cell shown in Fig. 1 is manufactured using existing fabrication technologies for polymer-based microfluidics. Kapton sheets (Dupont Inc.) and metallized Kapton sheets (Dunmore Corporation or Multek Inc.) are patterned via laser ablation. Metallized Kapton sheets are coated with 300 Å of aluminum

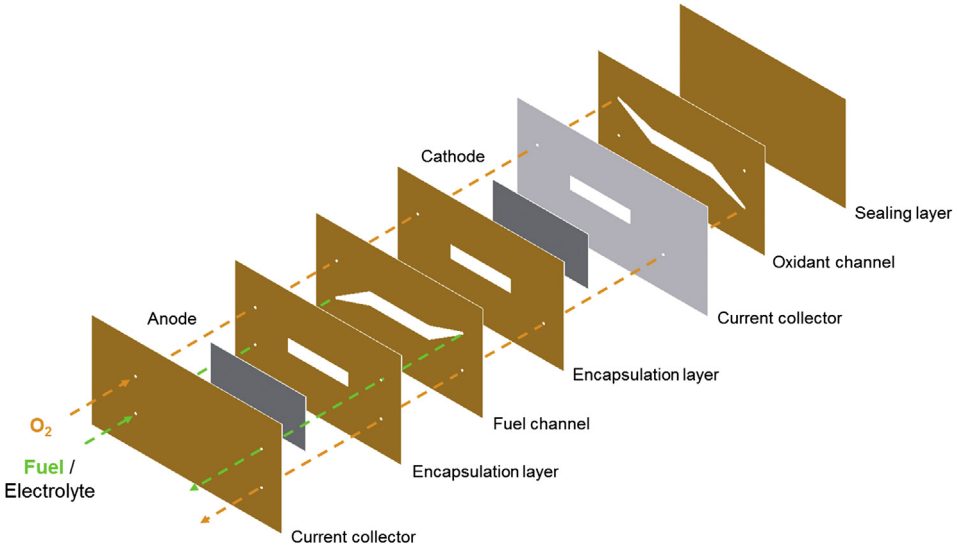

Fig. 1. Schematic of an all-polymer LFFC for manufacturing thin, lightweight fuel cell stacks. Anode and cathode layers are carbon paper, while other layers are laser-machined from Kapton (50 μm or 125 μm thick). Current collectors are Kapton layers that are metallized with aluminum to facilitate conduction of electrons. The fuel is methanol, the electrolyte is sulfuric acid, and the oxidant is oxygen.

(99.9% pure) on one side of the Kapton sheet. The metallized Kapton layers extend 0.5 inches beyond adjacent layers so that alligator clips from a potentiostat and a voltmeter can be electrically connected to electrodes. A silver epoxy (~150-μm thick) is deposited between carbon paper electrodes and metallized current collectors to improve electrical contact conductance. Nanoports (Upchurch Scientific Inc.) are bonded to the exterior surface of the fuel cell, using a two-part epoxy, to facilitate the entrance and exit of fuel/electrolyte and oxidant streams.

Bonding is a critical step in the fabrication of all microfluidic devices and in this polymer-based LFFC design, it is crucial to create strong bonding between polyimide layers. In this all-polymer LFFC, a heat-curing adhesive will be utilized in combination with an atmospheric plasma system to bond polyimide layers. The adhesive (EP41S-1, Master Bond Inc.) was chosen for its excellent chemical resistance to fuels as well as highly acidic environments, both of which are important for successfully sealing a laminar flow-based fuel cell. A 12-μm thick layer of adhesive is patterned between adjacent Kapton layers.

The atmospheric plasma system (Atomflo 250L, Surfx Technologies) is used to etch polyimide and increase the surface area for bonding [25–29]. The main advantage of an atmospheric plasma system over a traditional vacuum-based plasma system is that it does not require the use of a vacuum chamber. Atmospheric plasmas are operated at atmospheric pressure and can hence treat materials of any size. Furthermore, unlike vacuum-based plasma systems, atmospheric plasmas can be used to selectively treat part(s) of a material. Additionally, atmospheric plasmas are compatible with in-line manufacturing, unlike vacuum-based systems which require robotic assemblies to shuttle samples in and out of the vacuum chamber [30].

In this atmospheric plasma system (Atomflo 250L, Surfx Technologies), a secondary reactive gas (O_2) is added to a carrier gas (He) to reduce breakdown voltage. For this plasma treatment, ~2% O_2 gas is added to a helium-stabilized plasma; this concentration of O_2 is more than sufficient to etch/treat the surfaces of polymers, and because He has a breakdown voltage only 150 V, a high voltage transformer is not needed to operate this system [31,32]. The plasma system can be operated externally via LabView software, facilitating future integration with other manufacturing technologies.

A schematic of this fabrication procedure is shown in Fig. 2. Initially, polydimethyl-siloxane (PDMS, General Electric RTV 650) is prepared in a 10:1 ratio of monomer:crosslinker. The liquid PDMS prepolymer is vigorously mixed with the crosslinking agent and then degassed to remove any residual bubbles created during mixing. The degassed, polymer mixture is poured over a 4-inch silicon wafer and spun at 2000 rpm in a spin coater (SCS-G3P8, Specialty Coating Systems Inc.), resulting in a 25-μm thick layer of PDMS on the wafer. The coated wafer is then cured for ~20 min at 70 °C in a convection oven (VWR International).

At this time, a metallized Kapton layer is cleaned by first rinsing with acetone, water, isopropyl alcohol, and with water again. The metallized Kapton layer is dried under nitrogen and then plasma treated with an atmospheric plasma system (Atomflo-250L, Surfx Technologies). The plasma system is operated with a helium flow rate of 15.0 L min^{-1}, an oxygen flow rate of 0.2 L min^{-1}, and at a power level of 80 W. The metallized Kapton layer is translated ~1 cm below the stationary plasma head for ~20 s in a direction along the length of the layer and ~20 s in a direction along its width, ensuring that all areas of the metallized Kapton have been exposed to the plasma. Next, a two-part silver conductive epoxy (8331-14G, MG Chemicals) is deposited onto the aluminum side of the metallized Kapton layer. While aluminum is fine for this study in which fuel cells are only tested over shorter time periods, the order of days, metal coatings that are more resistant to fuel cell conditions should be used if these cells were intended for prolonged use. A mask is cut from weighing paper (Fisherbrand) to confine the Ag epoxy to the desired region for deposition and a knife blade is used to distribute the epoxy over the metallized Kapton surface. A catalyst-coated electrode is then placed on top of the silver epoxy.

Next, the PDMS-coated wafer is removed from the convection oven and allowed to cool for ~2 min. During this time, a Kapton

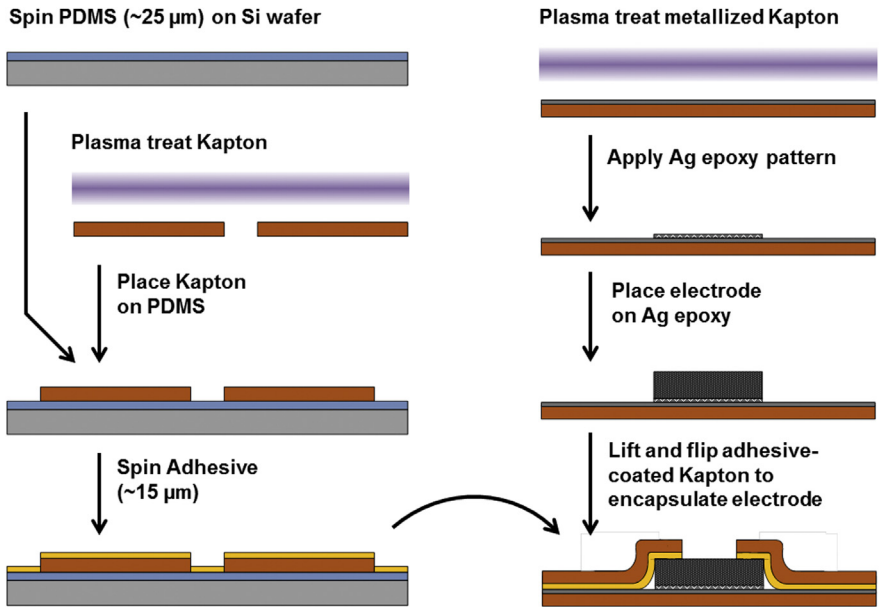

Fig. 2. Schematic which depicts the fabrication procedure for the all-polymer LFFC shown in Fig. 1. PDMS is spun onto a silicon wafer and a plasma-treated Kapton layer is placed onto the cured PDMS. Adhesive is spun over the entire Kapton layer. In parallel, metallized Kapton is plasma treated and a silver epoxy is deposited onto it. A carbon paper electrode is placed on the silver epoxy and the reversibly-bonded Kapton layer is then removed from the PDMS and used to encapsulate the electrode. Additional layers are added to the encapsulated electrode by repeating the four steps shown in the left column of this schematic.

channel layer is plasma treated at the same conditions as was done for the metallized Kapton layer. This Kapton channel layer is then placed on the PDMS-coated wafer, forming a reversible bond between the Kapton and PDMS. At this point, EP41S-1 is mixed (ARE-310, Thinky) at a 10:3 ratio of Part A:Part B for 6 min at 2000 rpm (mixing step) and 6 min at 2200 rpm (defoam step). The mixed EP41S-1 is then poured over the Kapton layer, which is reversibly-bonded to the PDMS-coated wafer, and spun at 8000 rpm in a spin coater. This spin rate results in a 12-μm layer of EP41S-1 on the Kapton layer. The reversibly-bonded Kapton layer is then peeled from the PDMS, leaving excess EP41S-1 on the PDMS-coated wafer.

Finally, the EP41S-1 coated Kapton layer is visually aligned and brought into contact with the catalyst-coated electrode that was previously adhered to the metallized Kapton layer. The adhesive is cured overnight at room temperature before any additional fabrication or testing is initiated. Additional Kapton channel layers can be added to the encapsulated electrode by repeating the procedure of depositing EP41S-1 onto a Kapton layer and then adhering the coated layer to the previously encapsulated electrode.

The fabrication process generally occurred as follows: (i) encapsulate both electrodes in Kapton, (ii) add a Kapton channel layer to the encapsulated anode, (iii) bond the encapsulated electrodes, (iv) add a Kapton channel layer to the cathode, and (v) enclose the exposed oxidant flow channel. Step (iii) is completed by spinning EP41S-1 onto the encapsulated cathode and bonding it to the encapsulated anode. A sacrificial layer of Kapton is cut to fit exactly in the window of the encapsulated cathode to prevent adhesive from being deposited on the exposed Nafion layer. After spinning adhesive, this sacrificial layer can easily be removed, leaving adhesive deposited only upon the Kapton which is encapsulating the cathode. Images of the cell at intermediate steps are shown in Fig. 3a–e. The complete cell shown in Fig. 3f is ~1 mm thick.

3.2. Electrode preparation

Unless specified otherwise, Pt/Ru/C (Alfa Aesar, 50:25:25 wt%) was used as the anode catalyst and Pt/C (Alfa Aesar, 50:50 wt%) was used as the cathode catalyst. The catalyst loading on the electrodes ranged from 2 to 3 mg cm^{-2}. The geometrical area of each electrode that is exposed to the electrolyte is 0.6×3.2 cm^2. So each electrode exposes about 2 cm^2 active catalyst area. Nafion (5 wt% solution, Ion Power Inc.) was added as a binder at a 20:3 ratio of catalyst to binder. Catalyst inks were prepared by mixing the desired amounts of catalyst and binder with 250 μL of Millipore water (18.1 MΩ) and 250 μL of isopropyl alcohol, which function as carrier solvents. The catalyst inks were sonicated (Sonics VCX-130PB) for 5 min to obtain a uniform mixture and were then hand-painted onto the microporous carbon-coated side of Sigracet 25BC (Fuel Cell Earth) carbon paper. Anodes were then hot-pressed (Carver 3851-0) at 1200 psi and 130 °C for 5 min to improve catalyst adhesion and electrode durability [19]. Anodes were placed catalyst side down onto a niobium foil to prevent the catalyst layer from attaching to the heated plates.

During the cathode hot-pressing procedure, a layer of Nafion 212 (Fuel Cell Earth) was placed on top of the catalyst layer before hot-pressing. This additional step resulted in a Nafion layer being bonded to each cathodic gas diffusion electrode (GDE) as a barrier to methanol crossover [19,33]. Nafion 212 was cleaned in a solution of 10 wt% nitric acid (Fisher) at 90 °C for 2 h and then stored in

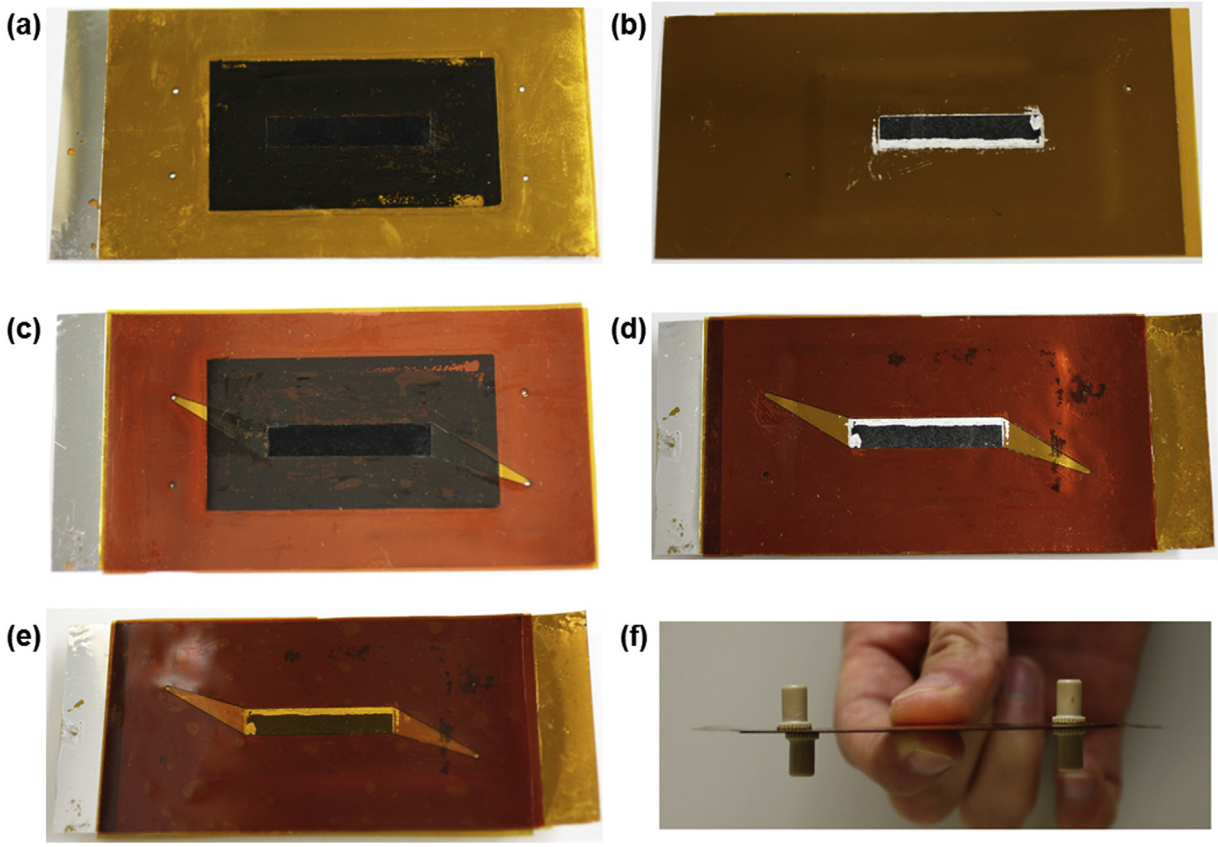

Fig. 3. Images of (a) a Kapton-encapsulated electrode with a 0.6×3.2 cm^2 electrode area, (b) the opening for oxygen to enter a Kapton cathode, (c) a Kapton anode with the fuel channel layer, (d) a Kapton cathode with the oxygen channel layer, (e) the backing layer bonded to a Kapton cathode, and (f) a complete Kapton-based LFFC.

Millipore water prior to the hot-pressing procedure. First, a damp layer of Nafion was placed onto a thin 4 in. × 3 in. Teflon sheet (0.005 in. thick, McMaster-Carr). The dampness of the layer ensured that it would stick flatly to the Teflon sheet. Cathodic GDEs were placed catalyst side down onto the Nafion layer and an additional layer of Teflon was placed on top of the GDE. The Teflon and cathode layers were then sandwiched between two aluminum plates and put into the hot-press at 1200 psi and 130 °C. Aluminum plates were rotated 90° every 1 min and 15 s to ensure even pressure distribution over the surface of the GDE. After 5 min, the aluminum plates were removed from the hot-press to yield a GDE with a Nafion layer bonded to it. This cathode hot-pressing procedure was optimized through iteration to ensure a uniformly flat cathode, which, in turn, ensures that adhesive is applied evenly over the surface of the Kapton cathode during the Kapton encapsulation process.

3.3. Fuel cell assembly

Prior to encapsulating electrodes in Kapton, studies were conducted in a microfluidic fuel cell setup that we developed earlier for catalyst and electrode characterization purposes [34–39]. An anode and a cathode were placed on either side of a 0.15-cm thick polymethyl-(methylacrylate) (PMMA) sheet, machined with a 3.3-cm long and 0.3-cm wide channel which enables the passage of fuel and electrolyte through the fuel cell during experimentation. Electrodes were placed facing inward on either side of the channel, such that the catalyst layer interfaces directly with the flowing stream. Two 0.1-cm thick, copper-infused graphite plates, with access windows (3.8 × 0.7 cm^2), were placed on the outside of the electrodes to serve as current collectors. Polycarbonate flow chambers (5.0 × 1.0 × 0.5 cm^3) were placed outside of the graphite windows for the introduction of gases. The multilayer assembly was held together using binder clips.

After electrodes had been encapsulated in Kapton, individual electrode studies were conducted with the complementary half of the microfluidic fuel cell platform. This half-Kapton, half-microfluidic fuel cell platform was assembled in the same manner as the traditional microfluidic fuel cell [34], and was held together with binder clips. After individual Kapton-encapsulated electrodes had been studied, a complete, all-polymer fuel cell was assembled by spinning EP41S-1 adhesive onto a Kapton-encapsulated cathode and then bonding it to a Kapton-encapsulated anode.

3.4. Fuel cell testing

Fuel cell experiments were conducted using NOVA Software (EcoChemie) controlled by a potentiostat (Autolab PGSTAT-30, EcoChemie). In the microfluidic fuel cell platform, oxygen and nitrogen gas (S.J. Smith, laboratory grade) are fed through the cathode and anode gas flow chambers, respectively, at a flow rate of 10 sccm (Cole Palmer). Nitrogen was introduced to the anode flow chamber to prevent oxygen otherwise present in the chamber from reacting on the Pt/Ru/C catalyst and thereby reducing fuel cell performance. A nitrogen supply was not needed for testing of Kapton-encapsulated anodes. The Kapton sheet sealed to their back prevents their contact with the surrounding atmosphere. For all experiments, the cell was supplied with a fuel stream consisting of 1 M methanol (Fisher) and 1 M sulfuric acid (H_2SO_4, GFS Chemicals), added for proton conduction. Fuel flow rates were held at 0.3 mL min^{-1} using a syringe pump (2200 PHD, Harvard Apparatus). All experiments were performed at room temperature. Once the gas and liquid streams were introduced, the fuel cell was held at open circuit potential (OCP) until the cell potential had stabilized.

A reference electrode (Ag/AgCl in saturated NaCl, BASi) was placed at the outlet of the fuel/electrolyte stream to enable independent analysis of polarization losses of each electrode. No potential drop is observed along the polyethylene tubing (Cole Parmer, 1.57 mm ID) connecting the fuel cell and the reference electrode [40]. Anode and cathode polarization losses were measured using two multimeters (15 XP Meterman, 87 III Fluke, or 179 Fluke), both grounded to the reference electrode, and attached to opposing graphite (or metallized Kapton) current collectors. Anode and cathode potentials, vs. the reference electrode, were used to determine the actual cell potential.

4. Results and discussion

After design, we first fabricated and tested individual anodes and cathodes in a microfluidic fuel cell setup to investigate individual electrode performance prior to Kapton encapsulation. Then electrodes were encapsulated in Kapton and re-tested in a half-Kapton, half-microfluidic fuel cell platform to quantify performance changes. Finally, Kapton-encapsulated electrodes are bonded together to evaluate the performance of a complete, all-polymer fuel cell.

4.1. Kapton-encapsulated anode characterization

One of the most important considerations when encapsulating electrodes in Kapton is ensuring good electrical contact between the electrode backing layer and the metallized Kapton current collector. As summarized in Fig. 4, the use of a silver epoxy improves electrical contact conductance between the anode backing layer and the metallized Kapton, thereby increasing performance at peak power density by ~224%. By hot-pressing the anode before using silver epoxy, the performance increases an additional ~21%. Hot-pressing does not impact the performance of anodes, and it reduces surface non-uniformities on the carbon paper that typically increase electrical contact resistance. The three Kapton anodes shown in Fig. 4 are loaded with Pt/Ru catalyst. Kapton cathodes were encapsulated using the same procedure as used for the anodes.

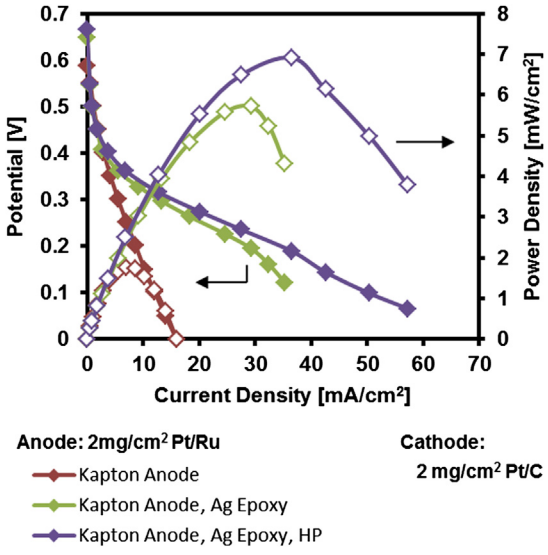

Fig. 4. Effect of silver (Ag) epoxy and hot-pressing on Kapton-encapsulated anode performance. Kapton-encapsulated anodes are tested in a novel half-Kapton, half-microfluidic fuel cell platform. Silver epoxy significantly lowers electrical contact resistance between anode backing layer and metallized Kapton current collector. Hot-pressing anodes further improves electrical contact between carbon paper and current collector.

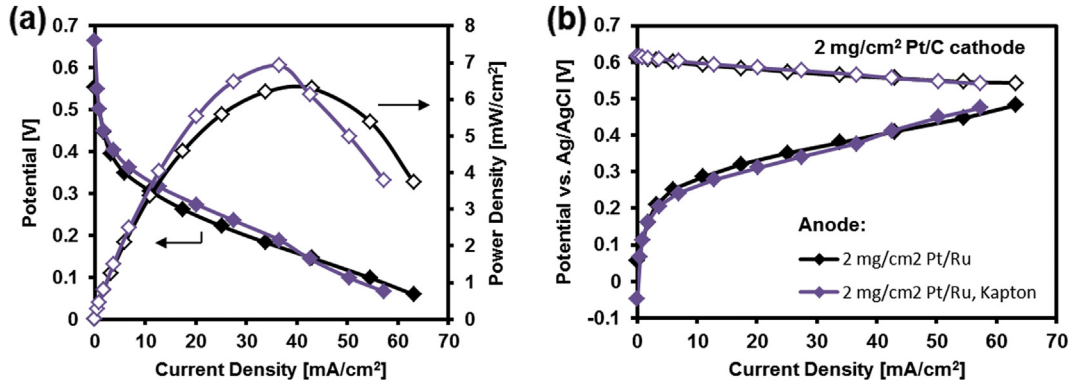

Fig. 5. Anode performance before and after Kapton encapsulation. Anode is initially tested in a microfluidic fuel cell platform and then re-tested in a half-Kapton, half-microfluidic fuel cell platform after Kapton encapsulation. (a) Polarization and power density curves show that peak power density remains constant when encapsulating anodes in Kapton and utilizing a silver epoxy between the anode and metallized Kapton current collector. Kapton encapsulation decreases the thickness of the anode half of our microfluidic fuel cell from 0.5-cm to 0.5-mm. (b) Corresponding individual electrode curves confirm that all performance changes occur at the anode.

Anodes are tested initially in a microfluidic fuel cell platform, and then retested after being encapsulated in Kapton to determine performance changes. Kapton anodes are ~0.5 mm thick, while the anode half of the microfluidic fuel cell platform is ~0.5 cm thick. Fig. 5 shows that this reduction in thickness does not decrease performance; up to peak power density, the Kapton-encapsulated anode performs slightly better than the same anode tested in a microfluidic fuel cell setup. Individual electrode curves (Fig. 5b) confirm that small performance changes can be attributed to the anode. At a cell potential of 0.25 V, the Kapton anode performs slightly better (~10%) than the same anode prior to Kapton encapsulation.

4.2. Kapton-encapsulated cathode characterization

Similar to Kapton-encapsulated anodes, Kapton-encapsulated cathodes are characterized using a half-Kapton, half-microfluidic fuel cell platform. These cathodes are tested initially in a microfluidic fuel cell platform, and then retested after being encapsulated in Kapton to determine performance changes. Kapton cathodes are ~0.5 mm thick, while the cathode half of the microfluidic fuel cell platform is ~0.5 cm thick. Fig. 6 shows that this reduction in thickness leads to minimal performance losses on the cathode. At peak power density, the cathode experiences an 11.9% decrease in performance due to Kapton encapsulation.

4.3. Complete cell studies

After individual electrodes are encapsulated in Kapton, complete all-polymer fuel cells are assembled by bonding Kapton anodes and Kapton cathodes. As shown in Fig. 7, the complete cell achieves 10.9 mW cm^{-2} when this specific anode and cathode are tested in a microfluidic fuel cell platform, whereas, after assembly of the complete polymer-based cell, performance is 9.7 mW cm^{-2}. So by transitioning from a 1-cm thick microfluidic fuel cell to a 1-mm thick all-polymer fuel cell, the performance drops by only 11%. Thus, a stack of ten all-polymer fuel cells will be as thick as our traditional microfluidic fuel cell, but will provide nine times as much power. The drop in performance observed for the complete cell is due to the decreased electrical contact conductance between electrodes and current collectors when encapsulating electrodes in Kapton, despite the use of silver epoxy in the assembly and encapsulation process. Individual electrode curves (Fig. 7b) show that the majority of polarization losses occur at the cathode due to the fact that cathode current collection only takes place along the edge of the active cathode area (oxidant window), whereas anode current collection also takes place within the anode catalyst area (solid backing). The complete cell reported here significantly outperforms prior work on polymer-based fuel microfuel cells operated using methanol as the fuel, *i.e.*, 10.9 mW cm^{-2} (our work) vs. <0.3 mW cm^{-2} [22]. This performance could probably be further

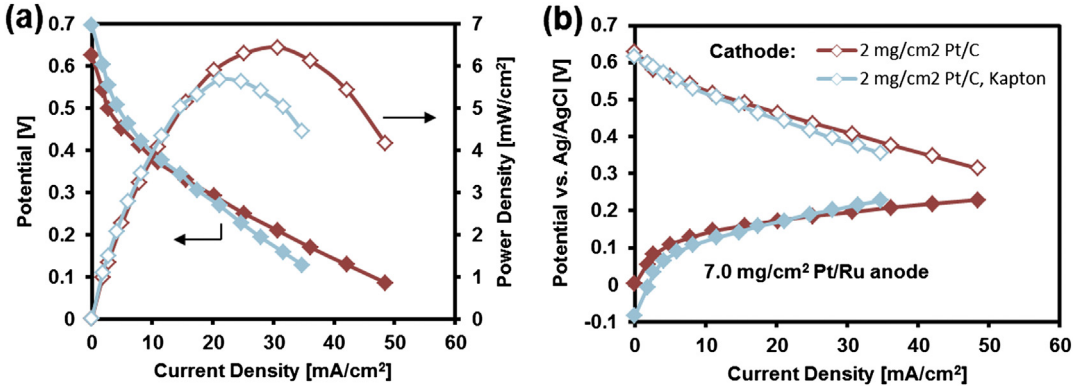

Fig. 6. Cathode performance before and after Kapton encapsulation. Cathode is initially tested in a microfluidic fuel cell platform and then re-tested in a half-Kapton, half-microfluidic fuel cell platform after Kapton encapsulation. (a) Polarization and power density curves before and after Kapton encapsulation. Peak power density decreases by ~10% due to encapsulating cathodes in Kapton and utilizing a silver epoxy between the cathode backing layer and the current collector, however, cell thickness decreases from 0.5 cm to 0.5 mm by encapsulating cathodes in Kapton. (b) Corresponding individual electrode curves for cathodes and Kapton-encapsulated cathodes, using the same 7.0 mg cm^{-2} Pt/Ru anode.

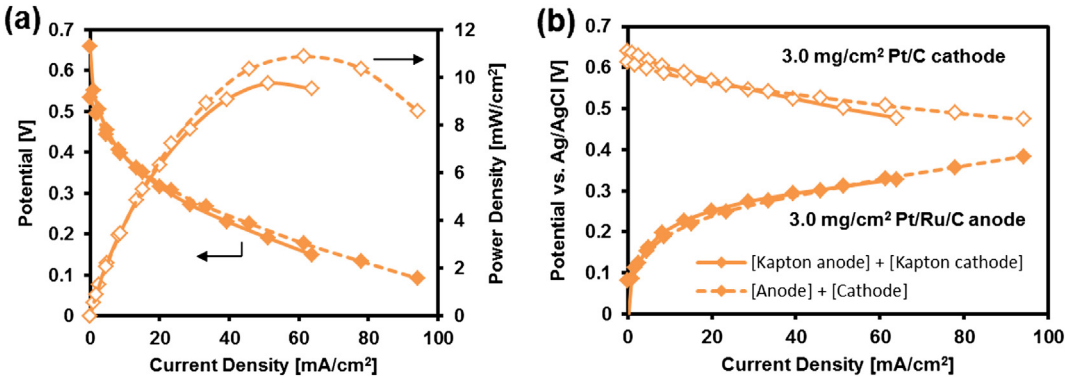

Fig. 7. Performance of a complete all-polymer fuel cell. (a) Polarization and power density curves for both electrodes before (dashed line) and after (solid line) Kapton encapsulation. This all-polymer fuel cell achieves ~10 mW cm^{-2} maximum power density. This all-polymer fuel cell is about 10 times thinner than the traditional microfluidic fuel cell, and achieves only ~10% less power. (b) Corresponding individual electrode curves show that the majority of polarization losses occur on the cathode.

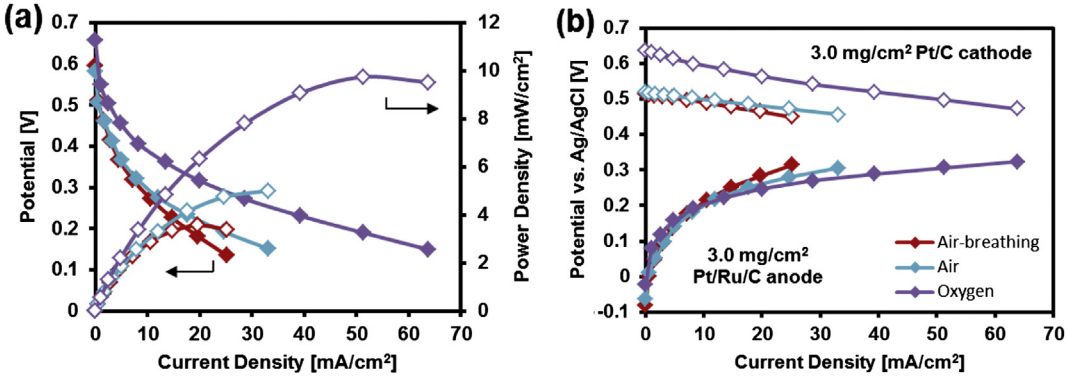

Fig. 8. Effect of oxidant on performance. (a) Polarization and power density curves for an all-polymer LFFC. Comparison of Kapton fuel cell performance when cathode is air-breathing, air supplied, and O_2 supplied shows that oxygen cathodes achieve ~70% higher performance than air cathodes. (b) Corresponding individual electrode curves show that cathode overpotential drops 0.1 V when using air instead of O_2.

improved by using more fuel cell tolerant materials (aluminum can degrade and/or its surface can be oxidized) and by ensuring the resistance of the metallized layer is negligible, so edge collection of current can be employed without performance penalty.

4.3.1. Performance as a function of oxidant

The fabrication process of a typical all-polymer LFFC occurred such that a Kapton cathode was bonded to a Kapton anode and then a Kapton oxidant flow chamber was added to the cathodic side of the cell. Before the Kapton flow chamber was added, the all-polymer cell was first tested with an air-breathing cathode. Once the cathodic Kapton flow chamber was added, the cell was tested again by supplying O_2 or air. The resulting polarization and power density curves for the complete all-polymer cell as a function of oxidant are shown in Fig. 8. Exposing the cathode to an air stream enhanced performance by ~30% over the air-breathing configuration. Performance increased by an additional ~70% upon flowing oxygen over the cathode as opposed to air. This performance increase is comparable to the 60% increase observed by Jayashree et al. when switching from an air stream to an oxygen stream in a formic acid LFFC [41]. Corresponding individual electrode curves (Fig. 8b) show that the cathode overpotential increases by 0.1 V when using O_2 instead of, air which accounts for the aforementioned performance improvements.

The complete, all-polymer cell was also tested as a function of cell orientation and fuel/electrolyte flow rate (0.3–1.5 mL min^{-1}), and the performance of the cell was found to be independent of both of these variables. The amount of water formed, or the orientation of the complete closed cell does not lead to different flow patterns and not to a redistribution of water within the cell. At the electrolyte flow rates used, it also does not affect the reference electrode measurement.

5. Conclusions

We have designed and fabricated a lightweight, Kapton-based fuel cell which is ~1 mm thick. Kapton has suitable bulk properties with respect to chemical resistance and thermal stability, and is relatively inexpensive to produce, making it a desirable polymer for a variety of applications. Here we laser machined Kapton layers to facilitate rapid prototyping of channel and encapsulation layers that are bonded via use of an adhesive and an atmospheric plasma system. Kapton-encapsulated anodes and cathodes were studied individually using a half-Kapton, half-microfluidic platform. These studies also show the importance of hot-pressing electrodes and of using a silver epoxy between the electrode backing layer and the metallized Kapton current collector to reduce contact resistance. The cell design reported here relies on edge collection of the current through a thin metallized layer, but this does not hamper performance. Minimizing contact resistance was much more important. Kapton-encapsulated anodes and cathodes experienced slight performance improvements and decreases, respectively, due to polymer-encapsulation. The complete, all-polymer fuel cell has been characterized as a function of oxidant and with a focus on the

performance changes associated with our alternative manufacturing approach.

The all-polymer fuel cell presented here will help to further the development of thin, lightweight fuel cell stacks for portable power applications. Automating the manufacture of this all-polymer cell will be important to future development efforts. For example, the deposition of silver epoxy could be automated using a transfer printing setup that has very high consistency and has been developed as a cost effective method for assembling micro-patterned structures such as solar cells [42]. Such a fully automated method would also allow for systematic investigation of silver epoxy layer thickness vs. performance. While EP41S-1 deposition is uniform, automated transfer printing could also be used to deposit EP41S-1 as a means of integrating fabrication steps. Fabrication times may be reduced by exploring curing the adhesive at elevated temperatures. In addition, scaling and stacking of this all-polymer fuel cell will improve the cell's potential as a power source for portable applications. Initial efforts should start with scaling to a multichannel design with manifolds. Upon successful scaling to a multichannel design, fuel cells can then be stacked to further increase power output. By stacking ten all-polymer LFFCs, the stack will be as thick as our traditional microfluidic fuel cells ($\sim$1.0 cm thick), but is expected to provide nine times as much power assuming power losses due to edge current collection can be minimized. Indeed, assembly and sealing of patterned polymer sheets is already being used for the manufacture of microfluidic platforms for a wide range of applications [43,44].

Now that we have shown the assembly and testing of an all-polymer fuel cell, several questions for subsequent research still remain: Will scaling to multi-channel arrays lead to performance loss due to edge current collection? Is the current amount of silver epoxy, and the currently used method of applying the silver epoxy, indeed leading to the best performance? This can be studied by systematically varying the amount applied, vs. conductivity in the resulting structures. Also, how much performance enhancement could be gained by using different designs and dimensions for the individual channels, inlets, and outlets? From our prior work [24] we know that shorter and wider channels lead to higher current densities in smaller space, and that introducing herringbone features in the top and bottom surfaces will lead to a better replenishment of the boundary layers. Will the all-polymer fuel cell designs in this study be amenable to such changes, and will the same factors of performance enhancement be observed?

Acknowledgments

We gratefully acknowledge financial support from the University of Illinois and the National Science Foundation through CAREER grant CTS 05-47617 as well as through awards CMMI 03-28162 and CMMI 07-49028 to Nano-CEMMS; a Nanoscale Science & Engineering Center (NSEC). The authors thank Larry Markoski (INI Power Systems, Morrisville, NC) for stimulating discussions.

References

[1] A. Manz, N. Graber, H.M. Widmer, Sensors and Actuators B Chemical B1 (1990) 244–248.
[2] K.F. Jensen, Chemical Engineering Science 56 (2001) 293–303.
[3] D. Erickson, D. Li, Analytica Chimica Acta 507 (2004) 11–26.
[4] L. Li, R.F. Ismagilov, Protein Crystallization Using Microfluidic Technologies Based on Valves, Droplets and SlipChip, in: D.C. Rees, K.A. Dill, J.R. Williamson (Eds.), Annual Review of Biophysics, vol. 39, 2010, pp. 139–158.
[5] R. Pal, M. Yang, R. Lin, B.N. Johnson, N. Srivastava, S.Z. Razzacki, K.J. Chomistek, D.C. Heldsinger, R.M. Haque, V.M. Ugaz, P.K. Thwar, Z. Chen, K. Alfano, M.B. Yim, M. Krishnan, A.O. Fuller, R.G. Larson, D.T. Burke, M.A. Burns, Lab on a Chip 5 (2005) 1024–1032.
[6] M. Toner, D. Irimia, Blood-on-a-chip, in: Annual Review of Biomedical Engineering, Annual Reviews, Palo Alto, 2005, pp. 77–103.
[7] C.C. Lee, G.D. Sui, A. Elizarov, C.Y.J. Shu, Y.S. Shin, A.N. Dooley, J. Huang, A. Daridon, P. Wyatt, D. Stout, H.C. Kolb, O.N. Witte, N. Satyamurthy, J.R. Heath, M.E. Phelps, S.R. Quake, H.R. Tseng, Science 310 (2005) 1793–1796.
[8] P. Yager, T. Edwards, E. Fu, K. Helton, K. Nelson, M.R. Tam, B.H. Weigl, Nature 442 (2006) 412–418.
[9] H. Becker, L.E. Locascio, Talanta 56 (2002) 267–287.
[10] A. de Mello, Lab on a Chip 2 (2002) 31N–36N.
[11] H. Becker, C. Gartner, Analytical and Bioanalytical Chemistry 390 (2008) 89–111.
[12] C.-W. Tsao, D.L. DeVoe, Microfluidics and Nanofluidics 6 (2009) 1–16.
[13] G.M. Whitesides, Nature 442 (2006) 368–373.
[14] E.R. Choban, L.J. Markoski, A. Wieckowski, P.J.A. Kenis, Journal of Power Sources 128 (2004) 54–60.
[15] J.L. Cohen, D.A. Westly, A. Pechenik, H.D. Abruña, Journal of Power Sources 139 (2005) 96–105.
[16] R.S. Jayashree, D. Egas, J.S. Spendelow, D. Natarajan, L.J. Markoski, P.J.A. Kenis, Electrochemical and Solid-State Letters 9 (2006) A252–A256.
[17] F.R. Brushett, R.S. Jayashree, W.-P. Zhou, P.J.A. Kenis, Electrochimica Acta 54 (2009) 7099–7105.
[18] E. Kjeang, N. Djilali, D. Sinton, Journal of Power Sources 186 (2009) 353–369.
[19] A.S. Hollinger, R.J. Maloney, R.S. Jayashree, D. Natarajan, L.J. Markoski, P.J.A. Kenis, Journal of Power Sources 195 (2010) 3523–3528.
[20] S.A.M. Shaegh, N.T. Nguyen, S.H. Chan, International Journal of Hydrogen Energy 36 (2011) 5675–5694.
[21] J. Wheldon, W.-J. Lee, D.-H. Lim, A.B. Broste, M. Bollinger, W.H. Smyrl, Electrochemical and Solid-State Letters 12 (2009) B86–B89.
[22] S. Tominaka, H. Nishizeko, J. Mizuno, T. Osaka, Energy and Environmental Science 2 (2009) 1074–1077.
[23] S. Metz, R. Holzer, P. Renaud, Lab on a Chip 1 (2001) 29–34.
[24] M.R. Thorson, F.R. Brushett, C.J. Timberg, P.J.A. Kenis, Journal of Power Sources 218 (2012) 28–33.
[25] J.Y. Jeong, S.E. Babayan, V.J. Tu, J. Park, I. Henins, R.F. Hicks, G.S. Selwyn, Plasma Sources Science & Technology 7 (1998) 282–285.
[26] J.Y. Jeong, S.E. Babayan, A. Schutze, V.J. Tu, J. Park, I. Henins, G.S. Selwyn, R.F. Hicks, Journal of Vacuum Science & Technology A 17 (1999) 2581–2585.
[27] M. Moravej, X. Yang, R.F. Hicks, J. Penelon, S.E. Babayan, Journal of Applied Physics 99 (2006).
[28] M.J. Shenton, M.C. Lovell-Hoare, G.C. Stevens, Journal of Physics D Applied Physics 34 (2001) 2754–2760.
[29] F.D. Egitto, L.J. Matienzo, IBM Journal of Research and Development 38 (1994) 423–439.
[30] A. Schutze, J.Y. Jeong, S.E. Babayan, J. Park, G.S. Selwyn, R.F. Hicks, IEEE Transactions on Plasma Science 26 (1998) 1685–1694.
[31] M. Moravej, X. Yang, G.R. Nowling, J.P. Chang, R.F. Hicks, S.E. Babayan, Journal of Applied Physics 96 (2004) 7011–7017.
[32] J. Park, I. Henins, H.W. Herrmann, G.S. Selwyn, Journal of Applied Physics 89 (2001) 15–19.
[33] E.H. Jung, U.H. Jung, T.H. Yang, D.H. Peak, D.H. Jung, S.H. Kim, International Journal of Hydrogen Energy 32 (2007) 903–907.
[34] R.S. Jayashree, M. Mitchell, D. Natarajan, L.J. Markoski, P.J.A. Kenis, Langmuir 23 (2007) 6871–6874.
[35] F.R. Brushett, W.-P. Zhou, R.S. Jayashree, P.J.A. Kenis, Journal of the Electrochemical Society 156 (2009) B565–B571.
[36] F.R. Brushett, A.S. Hollinger, L.J. Markoski, P.J.A. Kenis, in: ASME 2nd Micro/Nanoscale Heat & Mass Transfer International Conference, American Society of Mechanical Engineers, Shanghai, China, 2009, pp. 247–252.
[37] F.R. Brushett, H.T. Duong, J.W.D. Ng, R.L. Behrens, A. Wieckowski, P.J.A. Kenis, Journal of the Electrochemical Society 157 (2010) B837–B845.
[38] F.R. Brushett, M.S. Thorum, N.S. Lioutas, M.S. Naughton, C. Tornow, H.R. Jhong, A.A. Gewirth, P.J.A. Kenis, Journal of the American Chemical Society 132 (2010) 12185–12187.
[39] M.S. Naughton, F.R. Brushett, P.J.A. Kenis, Journal of Power Sources 196 (2011) 1762–1768.
[40] E.R. Choban, P. Waszczuk, P.J.A. Kenis, Electrochemical and Solid-State Letters 8 (2005) A348–A352.
[41] R.S. Jayashree, S.K. Yoon, F.R. Brushett, P.O. Lopez-Montesinos, D. Natarajan, L.J. Markoski, P.J.A. Kenis, Journal of Power Sources 195 (2010) 3569–3578.
[42] M.A. Meitl, Z.T. Zhu, V. Kumar, K.J. Lee, X. Feng, Y.Y. Huang, I. Adesida, R.G. Nuzzo, J.A. Rogers, Nature Materials 5 (2006) 33–38.
[43] S. Miserere, G. Mottet, V. Taniga, S. Descroix, J.L. Viovy, L. Malaquin, Lab on a Chip 12 (2012) 1849–1856.
[44] M. Focke, D. Kosse, C. Muller, H. Reinecke, R. Zengerle, F. von Stetten, Lab on a Chip 10 (2010) 1365–1386.